THE ASTRONOMICAL JOURNAL, 117:967–973, 1999 February

THE KINEMATICS OF POINT-SYMMETRIC PLANETARY NEBULAE

M. A. GUERRERO
Instituto de Astrofísica de Canarias, E-382000 La Laguna, Tenerife, Spain
R. VÁZQUEZ
Instituto de Astrofísica de Andalucía, CSIC, Apdo. 3004, E-18080 Granada, Spain
AND
J. A. LÓPEZ
Instituto de Astronomía, Universidad Nacional Autónoma de México, Apdo. Postal 877, 22800 Ensenada, B.C., Mexico
Received 1998 June 26; accepted 1998 October 12

ABSTRACT

Four planetary nebulae (PNe) with conspicuous point-symmetric morphology are studied in this paper through high-quality imagery and long-slit echelle spectroscopy. Point symmetry is also found in the velocity space, and this is related to particular forms of bipolar collimated outflows. Morphology and kinematics together reveal the presence of collimated bipolar ejections in an episodic way with indications of rotation or displacement of the symmetry axis of the outflow. Point symmetry is currently known to occur in a wide variety of PNe and the convenience of a reevaluation of point-symmetric PNe as a main morphological class is pointed out.

Key words: ISM: kinematics and dynamics —
planetary nebulae: individual (He 1-1, He 2-429, PC 19, Pe 1-17)

1. INTRODUCTION

Point symmetry in planetary nebulae (PNe) was formally introduced as a main morphological class by Corradi, Schwarz, & Stanghellini (1993) to distinguish those objects in the imaging catalog of Schwarz, Corradi, & Melnick (1992) that display relatively compact elliptical cores and prominent outer pairs of condensations disposed in point-reflection symmetry with respect to the geometrical nebular center. Gurzadyan (1969) had previously classified PNe with point-symmetric structures as "Sp" and "Sz," meaning spiral class and spiral class with a Z-shape, respectively.

The recent IAC Morphological Catalog of Northern Galactic Planetary Nebulae (Manchado et al. 1996) has revealed a number of previously unknown cases of PNe with point-symmetric morphology. There is an increasing number of objects, spanning nearly all the morphological groups and evolutionary stages in PNe, where point-symmetric structures are now apparent. In a number of cases in which detailed kinematic information is available, the presence of point-symmetric structures has been interpreted as originated by the action of a bipolar rotating episodic jet (BRET) (e.g., López, Meaburn, & Palmer 1993; López, Vázquez, & Rodríguez, 1995; López et al. 1997; López 1997). However, those that have been formally classified as point symmetric are included in the original catalog of Schwarz et al. (1992) and the IAC catalog (Manchado et al. 1996). These sources list four and eight objects, respectively. Surprisingly, out of these 12 objects only two, IC 4634 and He 2-186 (Schwarz 1993), have apparently been the subject of a kinematic investigation. Thus, there is obviously a pressing need to characterize them from a kinematic perspective.

The aim of this work is to initiate their detailed analysis for subsequent comparative and statistical studies. In this paper the following objects, Pe 1-17, PC 19, He 1-1, and He 2-429, classified as point symmetric in the IAC catalog, are analyzed. The last is classified as an elliptical with ansae but noted as containing point-symmetric extensions. All the objects in the sample have small angular sizes, less than 20″, and it is only due to the good-quality imagery and seeing conditions of the images presented that it is possible to discern some of the small ($<1''$), clumpy, localized regions of the point-symmetric structures within the nebular volume. The spatial resolution of the long-slit spectra, although more limited, has been adequate to distinguish the main relevant components for a detailed study of the spatio-kinematic characteristics of these objects.

2. OBSERVATIONS AND RESULTS

The images presented in this paper were obtained with the Nordic Optical Telescope (NOT) under the program for the IAC Morphological Catalog of Northern Galactic Planetary Nebulae (Manchado et al. 1996). The camera employs a 1024 × 1024 Thomson CCD. The pixel angular size scale as projected on the sky is 0.″139 pixel^{-1}. The FWHM of the stellar images in these frames is 0.″5 for Pe 1-17, 0.″6 for PC 19 and He 1-1, and 0.″7 for He 2-429. Figure 1 contains a mosaic of logarithmic gray-scale images of the objects studied here obtained through a filter centered on [N II] λ6584 with 10 Å FWHM. Insets at the corners show the main body of the nebula at low intensity levels in linear scale.

The long-slit echelle spectrometry was obtained also at the NOT with the IACUB spectrometer (McKeith et al. 1993) and the same Thomson CCD on the nights of 1997 July 22 and 23. A broad interference filter has been used to isolate the echelle order containing the Hα + [N II] lines. The slit length is 40″, which exceeds in all cases the angular size of the objects; 2 × 2 on-chip binning was set for the CCD, which yields a spatial resolution along the slit of 0.″278 pixel^{-1} and spectral dispersion of 0.094 Å pixel^{-1} ≡ 4.3 km s^{-1} pixel^{-1}. The spectral resolution as measured from the arc lines is ≃9–10 km s^{-1}. The spectra

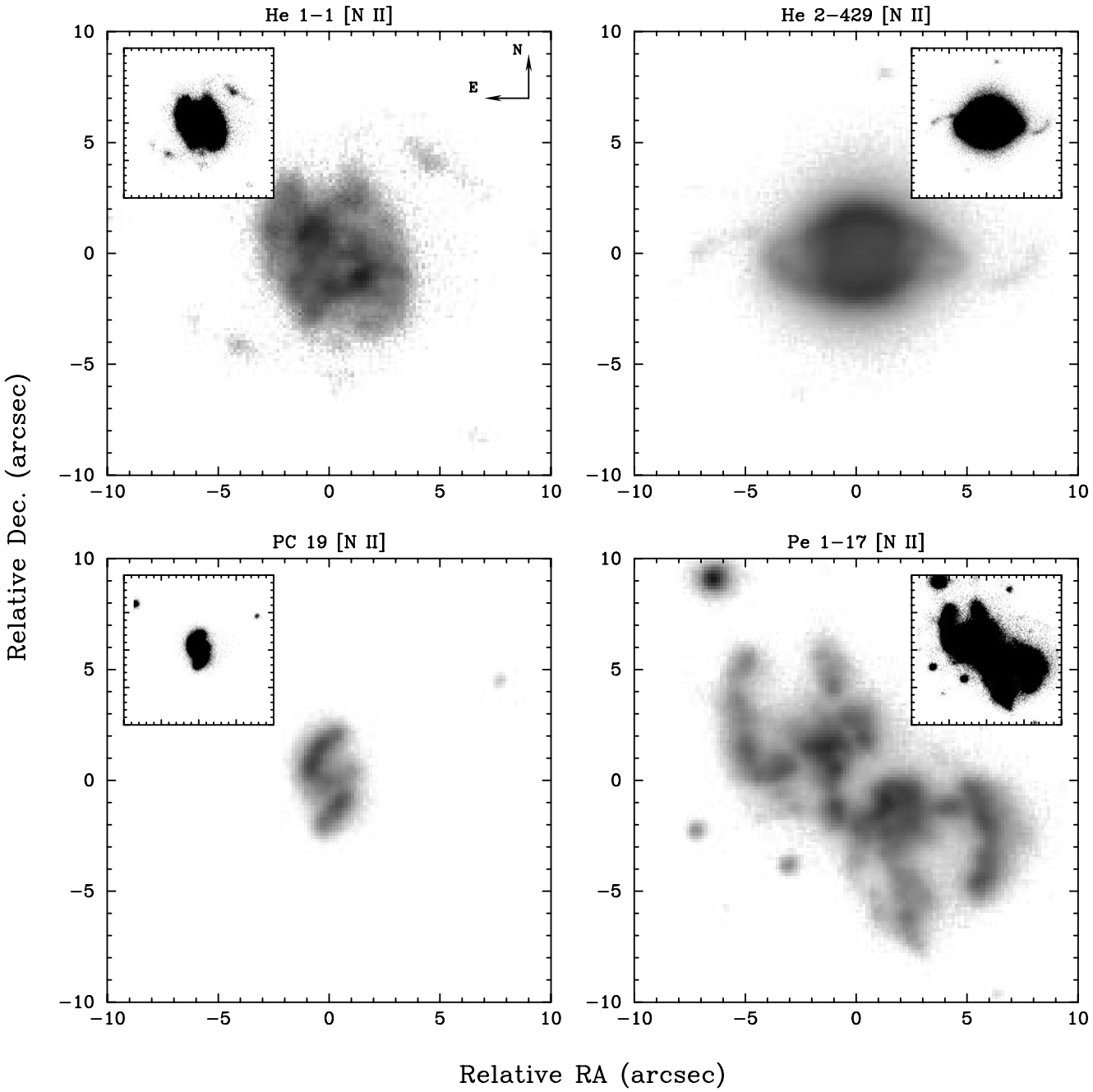

FIG. 1.—Logarithmic gray scale of the [N II] λ6584 images of He 1-1 (*top left*), He 2-429 (*top right*), PC 19 (*bottom left*), and Pe 1-17 (*bottom right*). The insets at the corners are displayed at low intensity levels in linear scale to emphasize the overall structure of each nebula. North is at the top, east to the left.

were reduced following standard procedures using IRAF.[1] In order to map the main velocity structures in the nebulae, several slit positions oriented at different position angles were obtained for each object. In Figure 2 the slit positions are indicated superposed on contour plots for each object. The slit width was set to 0″.64 in all cases; however, the seeing disk varied between 1″ and 1″.2 in this occasion.

The resultant spectra for each object are shown in Figures 3–6. The angular size scales are equal throughout all the figures, images, and spectra.

3. DISCUSSION

3.1. *Morphology*

The macrostructure of He 1-1, He 2-429, and PC 19 (see the insets in Fig. 1) are mainly elliptical; however, their detailed individual characteristics are notoriously different, as shown in the logarithmic representations of the main panels in Figure 1. They are summarized briefly. He 1-1 is dominated by an inner expanding ring aligned perpendicular to the outflow axis of the point-symmetric filaments, reminiscent of the case of Fleming 1 (López et al. 1993;

[1] IRAF is distributed by the National Optical Astronomy Observatories, which are operated by the Association of Universities for Research in Astronomy, (AURA), Inc., under cooperative agreement with the National Science Foundation.

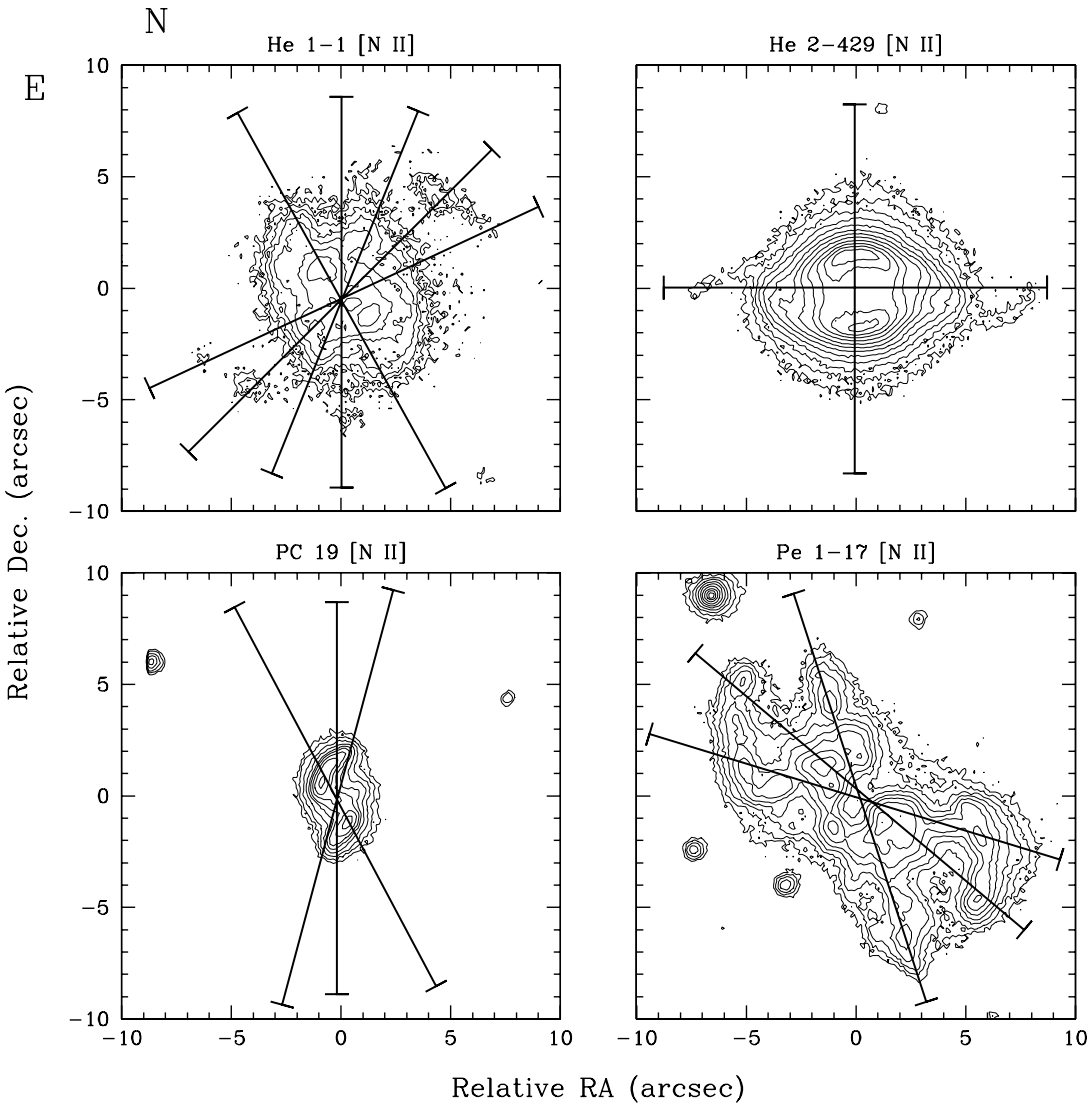

FIG. 2.—Slit positions over which spectral information was obtained are indicated on the contour maps of the [N II] images of He 1-1 (*top left*), He 2-429 (*top right*), PC 19 (*bottom left*), and Pe 1-17 (*bottom right*). The contours are separated by a factor 1.7 in intensity, with the first contour at the 3 σ level. The slit width convolved with the disk seeing is represented by the line cap width.

Palmer et al. 1996). He 2-429 has an open-ended, elliptical shell in whose extremes, nearly perfect point-symmetric filaments emerge. The morphological similarity of this object with the three-dimensional MHD models of García-Segura (1997) is striking. Contrary to the two former cases, in which the point-symmetric filaments extend beyond the main body of the PN, in the case of PC 19 the point-symmetric arcs are contained within the elliptical shell, similar to the cases of Cn 3-1 (Miranda et al. 1997) and K 3-35 (Miranda et al. 1998), and no inner ring is detected. On the other hand, Pe 1-17 represents a highly peculiar case, with a macrostructure that is rather bipolar, even with hints of a waist, which is an exception to the description of point-symmetric PNe given by Schwarz (1993). Its inner clumpy structure has revealed the most extreme and complex case of point symmetry known so far.

3.2. *Kinematics*

He 1-1.—Five slit positions oriented at different position angles (29°, 0°, 337°.5, 315°, and 295°) were obtained over this nebula to study its kinematics. The corresponding [N II] λ6584 line profiles are shown in Figure 3. The heliocentric velocity expansion of the bright inner ring increases with position angle, being lowest at P.A. 29° and highest at P.A. 295°, with $V_{\rm exp}$ values ranging from $\approx$33 km s^{-1} to 47 km s^{-1}, respectively. Given that the point-symmetric filaments are oriented along position angles between 315° and 295°, this indicates the presence of a bipolar outflow along this direction. The heliocentric velocities observed in the two main clumps of the point-symmetric filaments are +11 km s^{-1} and −5 km s^{-1} in the northwest and −76 km s^{-1} and −68 km s^{-1} in the southeast. A remarkable property of this bipolar outflow is that the outer point-symmetric filaments conserve the velocity of the corresponding expanding component of the inner shell from which they emerge. This effect is apparent in the P.A. 315° and 295° slit profiles in Figure 3.

He 2-429.—Two slit positions at P.A. 0° and 270° were observed on He 2-429 to study its kinematics. The slit at P.A. 0° shows the spectrum from an ellipsoidal shell, see Figure 4, with an expansion velocity $V_{\rm exp}$ = 30 km s^{-1}.

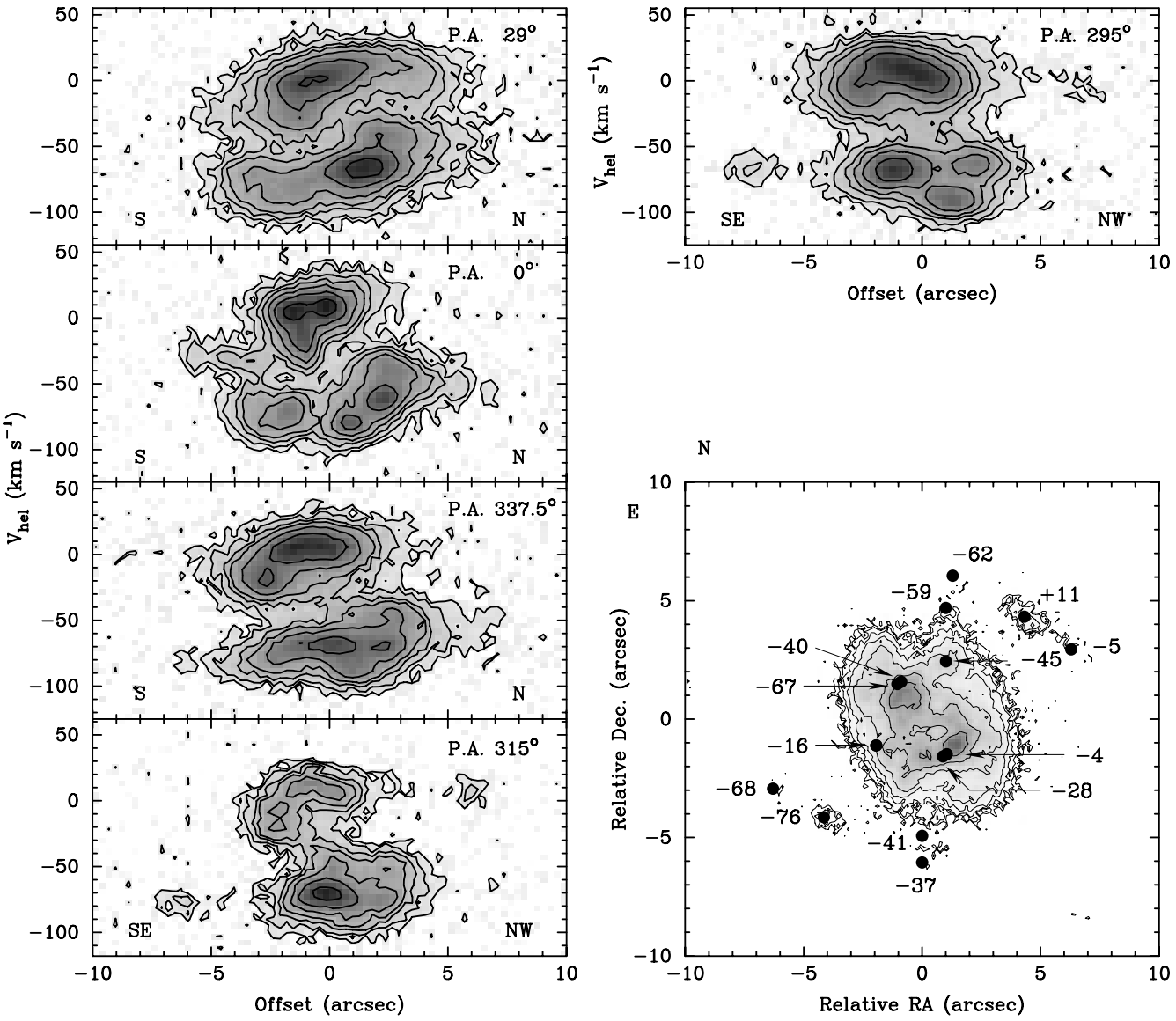

FIG. 3.—Gray-scale representation with contour maps of the echellograms and image of He 1-1 in the [N II] λ6584 emission line. Both the direct image and spectra are shown at the same spatial scale. The line profiles are shown as velocity position maps using a square root transformation of the gray-scale levels. The contours are separated by a factor 2.0 in intensity, with the first contour at the 4.5 σ level for clarity. The observed radial velocities have been converted to the heliocentric system. The corresponding slit orientations are indicated. Some representative heliocentric velocity points are indicated over the contour plot of the nebula.

Velocity splitting decreases outward from the center toward a systemic velocity of $+30$ km s^{-1}.

The slit at P.A. 270° shows the expected kinematic behavior along the major axis of the ellipsoid, although emission along the borders decreases toward the outer zones. The point-symmetric filaments are faint but discernible along this slit. They show a slight curvature in the velocity space, particularly the eastern filament with positive velocities increasing outward on this side and just a trace of the opposite behavior in the western side. Mean velocities at the tips of the extensions are close to systemic with values of $+26$ km s^{-1} (east) and $+32$ km s^{-1} (west). The morphology and kinematics of He 2-429 indicate that the major axis of the ellipsoid is tilted only $\approx 3°$ with respect to the plane of the sky.

PC 19.—Three different slit positions were obtained over PC 19. The corresponding [N II] λ6584 line profiles are shown in Figure 5; the contour map with representative heliocentric velocities shown in this same figure indicates expansion velocities increasing toward the outer regions of the arclike filaments. In this sense, velocity differences range from 61 to 70 km s^{-1} or their halves in terms of expansion. The heliocentric systemic velocity is -10 km s^{-1}; thus, with respect to the object's reference frame, outflow velocities are of the order of 20 to 25 km s^{-1}.

Pe 1-17.—The kinematics of Pe 1-17 (Fig. 6) is as unusual as its morphology. Slits at P.A.s 18°.5, 50°, and 253° (73°) were recorded. The two central condensations are expanding at a rate of 24 km s^{-1} with respect to each other; the bright knot to the northeast of the geometrical center has a $V_{Hel} = +32$ km s^{-1} and the one to the southwest a dominant component at $V_{Hel} = -16$ km s^{-1}. The latter is also seen split into two well-defined velocity components in the P.A. 18°.5 slit, with the positive component at $V_{Hel} = +40$

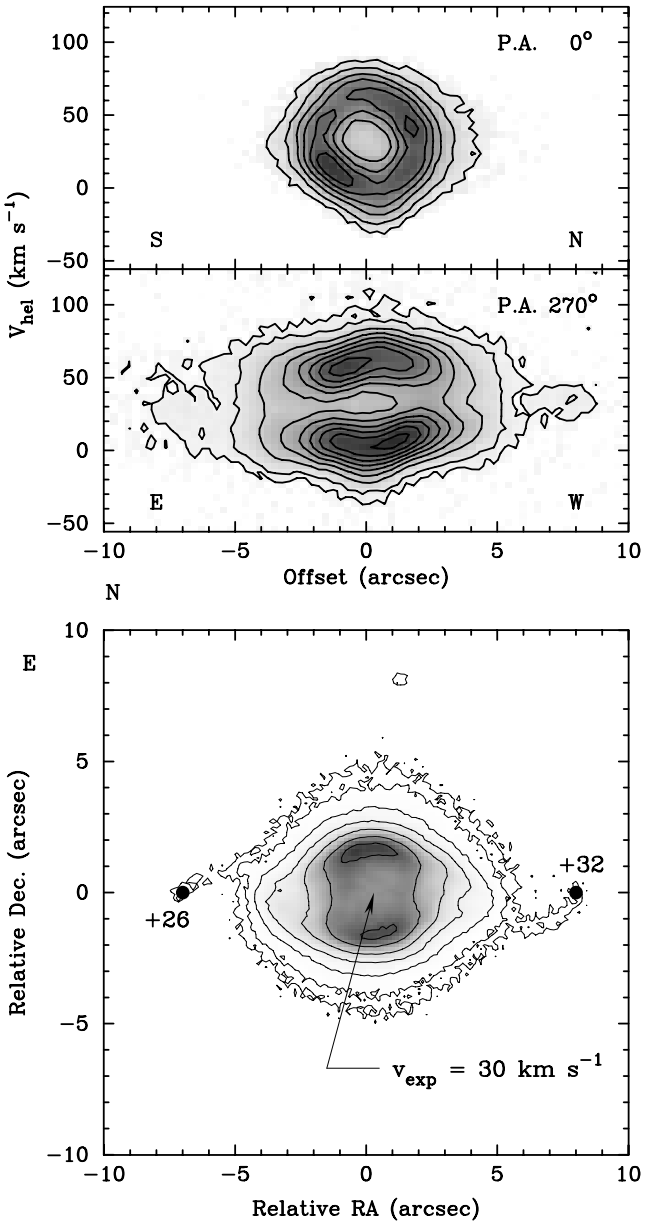

FIG. 4.—Same as Fig. 3, but for He 2-429

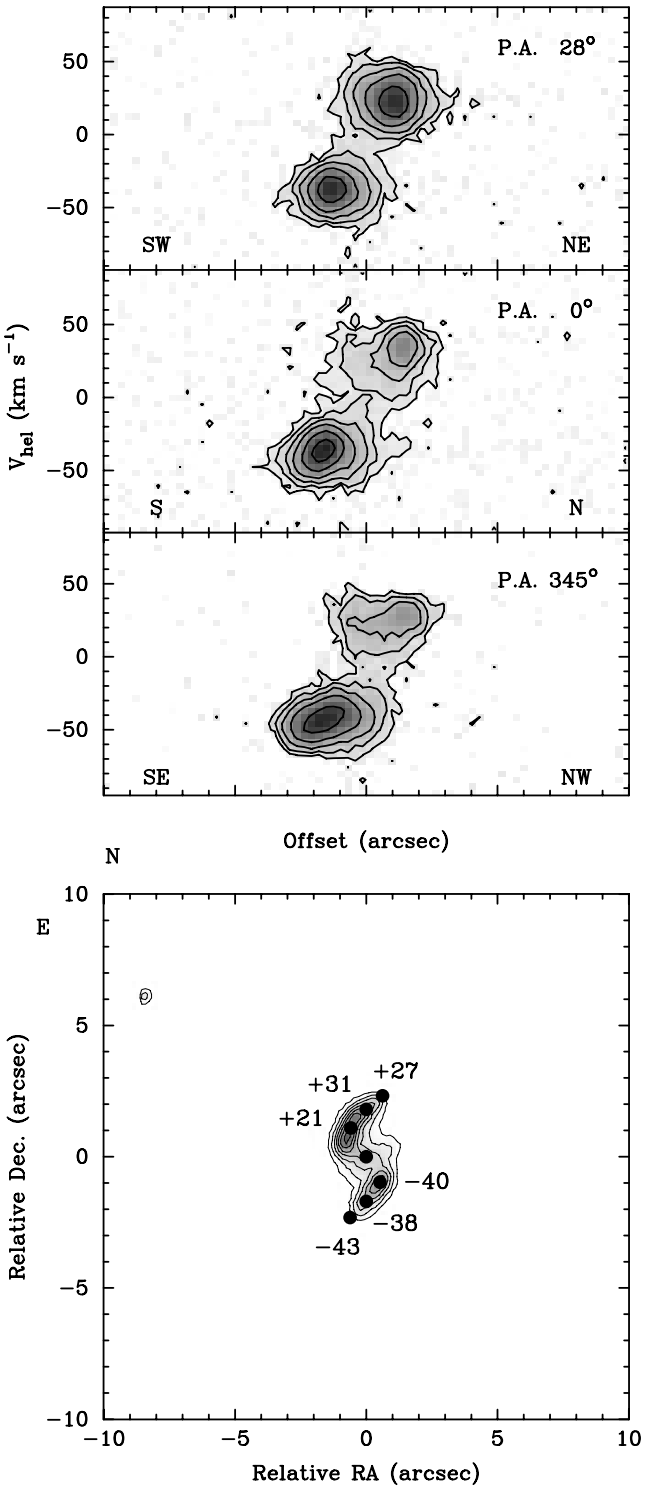

FIG. 5.—Same as Fig. 3, but for PC 19

km s^{-1}. Clear velocity splitting is traced along this position angle extending to the southern side of the slit where V_{Hel} components of +41 km s^{-1} and −6 km s^{-1} are observed, resembling an expanding lobe. On the opposite northern side of this slit the positive V_{Hel} component tends to a value of +23 km s^{-1}, the corresponding negative component (−12 km s^{-1}) is much fainter in this region. A simplistic interpretation of the overall kinematics along this P.A. 18°.5 slit could be that of an expanding, elongated shell with intensity maxima marked by the also expanding bright condensations.

The slits at P.A.s 50° and 253° also cross over the central bright knots. Splitting is also detected over the central region, but this is not evident along the other regions covered by these slits, which indicates that the expanding elongated shell is highly localized along the PA 18°.5 slit and particularly in the southwest side. These slits map different segments of the twisted armlike nebular extensions. On the 50° slit the northeast and southwest tips of the filaments show V_{Hel} of +8 and +19 km s^{-1}, respectively. At the "elbows" of these armlike filaments, covered by the P.A. 253° slit, sharp velocity contrasts are found, and these are directed in the opposite sense to the velocity expansion of the corresponding bright central knot to which they seem connected. The general kinematic behavior cannot be accommodated within a simple perspective. The global picture reveals two bright expanding condensations and highly collimated outflows composed of seemingly episodic

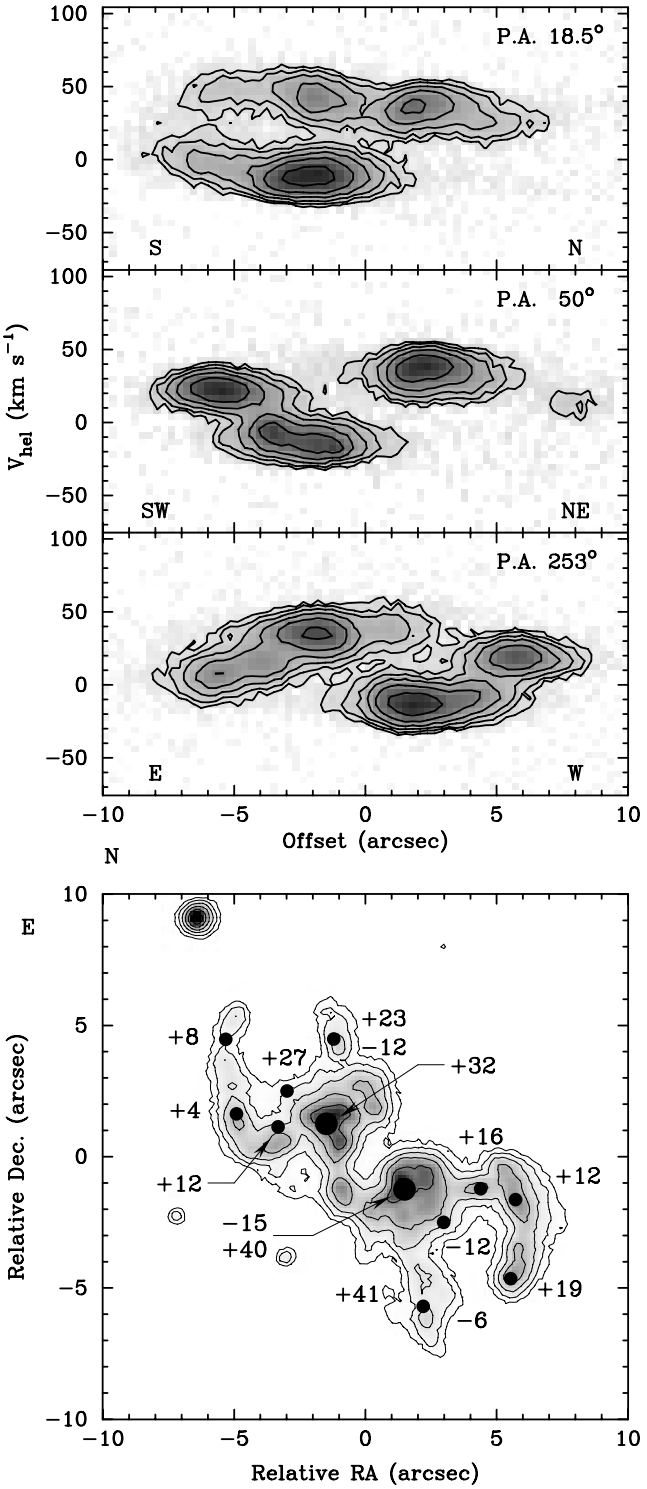

FIG. 6.—Same as Fig. 3, but for Pe 1-17

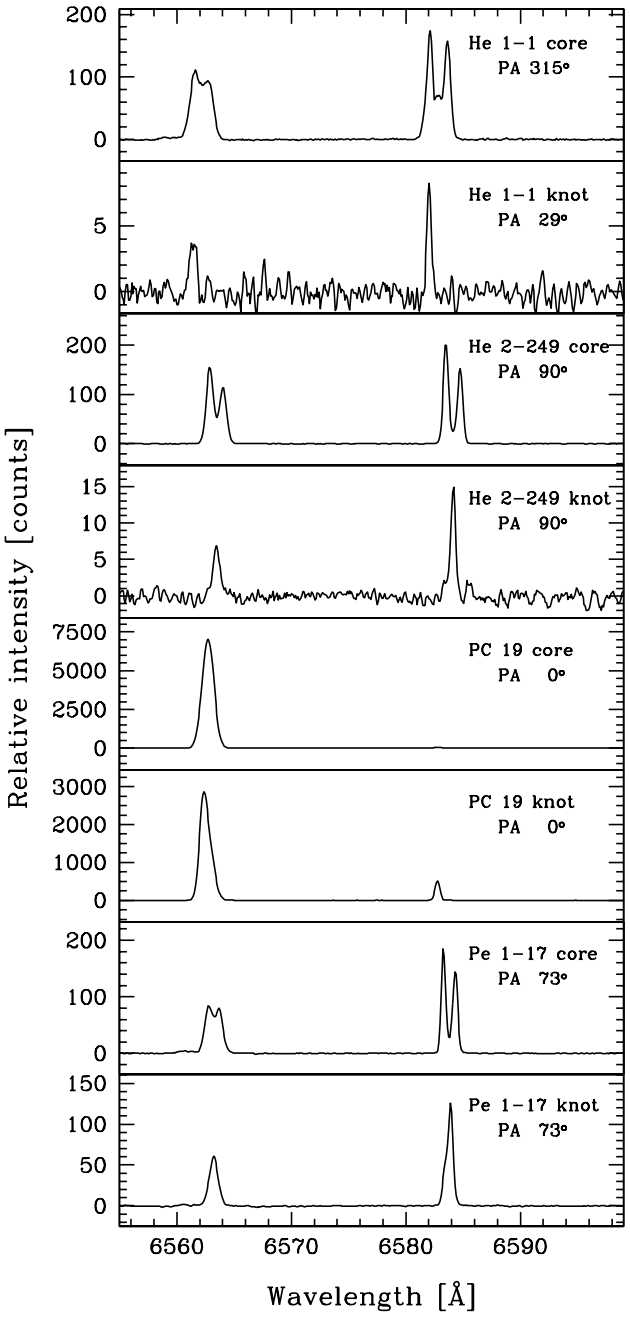

FIG. 7.—Representative integrated spectra in the range of Hα and [N II] over the central regions and selected point-symmetric components (knots) for the four PNe under study.

ejections followed by changes in direction of the symmetry axis of a most complex nature. No traces of the central star are apparent in any of the narrow band images, nor in the long-slit spectra; thus its location at this time can only be speculated to lie somewhere near the center of the whole structure.

3.3. *Line Ratios*

A mosaic of integrated spectra is presented in Figure 7, where Hα/[N II] ratios for the core and a representative outer region for each of the four nebulae can be appreciated. The dominance of [N II] λ6584 over Hα is apparent in all the objects except for PC 19. More relevant is the fact that the [N II]/Hα ratios are all enhanced in the knots as compared to their cores (by a factor of 1.12 in the case of He 1-1; 11.23 for PC 19; 1.35 for He 2-429; and 1.21 for Pe 1-17). In the case of PC 19, the [N II]/Hα ratio is extremely low in the core and shows the largest proportional enhancement in the outer regions.

Nebular ionic abundances are available for He 1-1, Pe 1-17 (Samland et al. 1992), and PC 19 (Cuisiner, Acker, & Köppen 1996). In none of these cases the N abundance is found to be enhanced. Also, given the moderate outflow velocities derived here, the presence of strong shocks that

may contribute significant collisional excitation over photoionization processes in the PN environment is unlikely (e.g., Dopita 1997). These characteristics are similar to those found in fast low-ionization emission regions (Balick et al. 1998).

3.4. *Point Symmetry as a Class*

The discovery rate of collimated outflows and point-symmetric features in PNe has proliferated during the last few years, undoubtedly due to the availability of higher quality data. Their analysis has reinforced the notion that point symmetry reflects the presence of collimated, bipolar outflows indicative of episodic mass ejections; albeit, in higher proportions than previously expected, and its occurrence does not seem to be restricted to a particular main morphological class. For example, point-symmetric features in PNe are now being found in a wide range of dissimilar PNe, from bipolars with huge extensions such as KjPn 8 (López et al. 1995) to compact, very young ones such as He 3-1475 (Borkowski, Blondin, & Harrington 1997) and peculiar cases such as NGC 6543 (Miranda & Solf 1992). Additional evidence in this regard has also come recently from the *Hubble Space Telescope* images obtained by Sahai & Trauger (1998) of very low excitation, young PNe in which point symmetry is outstanding within a diversity of aspherical shapes. Futhermore, some bipolars like M2-9 and Hb 5 also contain prominent point-symmetric structures in their lobes, and it is interesting to note that contrary to the moderate outflow velocities of the sample studied here, bipolar PNe usually show high ($\gtrsim 100$ km s^{-1}) expansion velocities (e.g., Corradi & Schwarz 1995).

The diversity of conditions under which point symmetry seems to be generated precludes at this time the interpretation of their formation within a unified dynamical model. Schwarz (1993) and Livio & Pringle (1996) have suggested the presence of accretion disks produced by binary nuclei, where precession or warping instabilities of the disk, respectively, would produce the point symmetry in the bipolar outflow. However, the key observations that would allow to test the models beyond the convincing arguments of their likely influence in some point-symmetric PNe are still lacking.

4. CONCLUSIONS

Four point-symmetric planetary nebulae are studied in this paper via high-quality ground-based imagery and high-resolution long-slit spectroscopy. Three of them show mainly elliptical macrostructures, while the fourth is basically bipolar. Their detailed characteristics or microstructure are notoriously different among each other, making it difficult to infer a common mechanism in the production of their collimated outflows at this stage.

Pe 1-17 is notable as it is the most remarkable and complex known case of point symmetry in PNe.

The kinematics shows that the morphology is reflected in the velocity space, indicating that point-symmetric features are indeed related to particular forms of bipolar, collimated outflows involving episodic mass ejection and displacement or rotation of the symmetry axis. Expansion velocities for the objects studied are in the range of 30 km s^{-1} to 50 km s^{-1}.

[N II]/Hα intensity ratios are found to be enhanced in the outer point-symmetric filaments and knots compared to the central regions.

The presence of point-symmetric microstructures do not seem to be correlated with a particular main morphological class. Therefore, a reevaluation of the definition of the point-symmetric class in PNe seems necessary.

This work is partially based on observations made with the Nordic Optical Telescope, operated on the island of La Palma by the Lund Observatory in the Spanish Observatory del Roque de Los Muchachos of the Instituto de Astrofísica de Canarias. M. A. G. gratefully acknowledges funding through grant PB94-1274 from the Dirección General de Investigación Científica y Técnica of the Spanish Ministerio de Educación y Ciencia and the hospitality of the IAUNAM-Ensenada during a visit related to this work. R. V. is in grateful receipt of a graduate scholarship from the AECI (Spain), complementary support from DGAPA-UNAM (Mexico), and partial support by DGICYT grant PB95-066 and the Junta de Andalucía (Spain). J. A. L. acknowledges the continuous financial support from DGAPA-UNAM through projects IN 111896 and IN 101495. The authors gratefully acknowledge L. F. Miranda and R. L. M. Corradi for helpful discussions and assistance with the IACUB-Echelle observations at the NOT, respectively.

REFERENCES

Balick, B., Hajian, A. R., Terzian, Y., Perinotto, M., & Patriarchi, P. 1998, AJ, 116, 360
Borkowski, K. J., Blondin, J. M., & Harrington, J. P. 1997, ApJ, 482, L97
Corradi, R. L. M., & Schwarz, H. E. 1995, A&A, 293, 871
Corradi, R. L. M., Schwarz, H. E., & Stanghellini, L. 1993, in IAU Symp. 155, Planetary Nebulae, ed. R. Weinberger & A. Acker (Dordrecht: Kluwer), 216
Cuisinier, F., Acker, A., & Köppen, J. 1996, A&A, 307, 215
Dopita, M. A. 1997, ApJ, 485, L41
García-Segura, G. 1997, ApJ, 489, L189
Gurzadyan, G. A. 1969, Planetary Nebulae (New York: Gordon Breach)
Livio, M., & Pringle, J. E. 1996, ApJ, 465, L55
López, J. A., Meaburn, J., Bryce, M., & Rodríguez, L. F. 1997, ApJ, 475, 705
López, J. A., Meaburn, J., & Palmer, J. W. 1993, ApJ, 415, L135
López, J. A., Vázquez, R., & Rodríguez, L. F. 1995, ApJ, 455, L63
López, J. A. 1997, in IAU Symp. 180, Planetary Nebulae, ed. H. J. Habing & H. J. G. L. M. Lamers (Kluwer: Dordrecht), 197
Manchado, A., Guerrero, M. A., Stanghellini, L., & Serra-Ricart, M. 1996, in The IAC Morphological Catalog of Northern Galactic Planetary Nebulae (La Laguna: IAC)
McKeith, C. D., García-López, R., Rebolo, R., Barnett, E. W., Beckman, J. E., Martín, E. L., & Trapero, J. 1993, A&A, 273, 331
Miranda, L. F., & Solf, J. 1992, A&A, 260, 397
Miranda, L. F., Torrelles, J. M., Guerrero, M. A., Aaquist, O. B., & Eiroa, C. 1998, MNRAS, 298, 243
Miranda, L. F., Vázquez, R., Torrelles, J. M., Eiroa, C., & López, J. A. 1997, MNRAS, 288, 777
Palmer, J. W., López, J. A., Meaburn, J., & Lloyd, H. M. 1996, A&A, 307, 225
Sahai, R., & Trauger, J. T. 1998, AJ, 116, 1357
Samland, M., Köppen, J., Acker, A., & Stenholm, B. 1992, A&A, 264, 184
Schwarz, H. E., Corradi, R. L. M., & Melnick, J. 1992, A&AS, 96, 23
Schwarz, H. E. 1993, in Mass Loss on the AGB and Beyond, ed. H. E. Schwarz (Garching: ESO), 223